



available at www.sciencedirect.com



journal homepage: www.elsevier.com/locate/carbon



The simultaneous reduction of nitric oxide and soot in emissions from diesel engines

Markus Sander^a, Abhijeet Raj^a, Oliver Inderwildi^a, Markus Kraft^{a,*},
Sven Kureti^b, Henning Bockhorn^b

^aDepartment of Chemical Engineering, University of Cambridge, Pembroke Street, Cambridge CB2 3RA, UK

^bInstitut für Technische Chemie und Polymerchemie Universität Karlsruhe, 76128 Karlsruhe, Germany

ARTICLE INFO

Article history:

Received 15 July 2008

Accepted 23 November 2008

Available online 6 December 2008

ABSTRACT

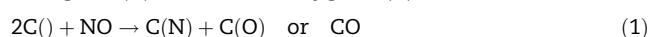
Recent studies demonstrate that the decomposition of nitric oxide on a soot molecule forms surface nitrogen and oxygen. The surface nitrogen can be recombined to gaseous N₂ while the surface oxygen desorbs from the soot molecule as CO. This non-catalytic conversion of gaseous NO into N₂ is investigated using density functional theory, transition state theory and a kinetic Monte-Carlo (kMC) simulation. The results are validated against experiments. A mechanism for the conversion of NO to N₂ on a soot surface is explored. The geometries of the intermediate stable species as well as the transition states were optimized to identify the different reaction steps. The forward and backward reaction rate of each intermediate reaction is calculated applying transition state theory. A kMC simulation using the current rates and intermediate species demonstrates feasible mechanisms for the conversion of NO to N₂ on a soot surface. It is also suggested that a portion of NO is trapped on the soot surface and this increases during the reaction and blocks the active carbon sites inhibiting further reactions. By combining different theoretical techniques in a multi-scale model, we are able to describe the conversion of soot in the presence of NO accurately.

© 2008 Elsevier Ltd. All rights reserved.

1. Introduction

Diesel exhaust contains many harmful substances including soot, NO_x and CO. The removal of these pollutants is thus important for the environment and consequently for human health. The reduction of soot and NO_x has been investigated by many researchers and most of the studies published in this area have investigated the removal of either NO_x or soot from the exhaust gas. Diesel particulate filters are the most favored exhaust treatment to reduce soot whereas NO_x storage catalysts are preferred to abate NO_x. Twigg summarizes these exhaust-gas aftertreatment techniques in a recent review [1]. The reduction of NO_x has mainly been studied in the presence of catalysts [2–5], however, the direct interaction between soot and NO_x can also remove both substances simulta-

neously. This direct non-catalytic reaction between nitrogen oxide and soot is studied in [6–12]. In most of these studies the hydrogen atoms have been removed from the soot by oxygen to create free radical carbon sites, denoted as C(). NO attaches to two neighboring active carbon sites forming surface nitrogen C(N) and surface oxygen C(O)



The surface nitrogen C(N) recombines to N₂ as suggested by [8,9,20,21]:



Illán-Gómez et al. have also investigated the reduction of NO on activated carbon sites concerning also the catalytic

* Corresponding author:

E-mail address: mk306@cam.ac.uk (M. Kraft).

0008-6223/\$ - see front matter © 2008 Elsevier Ltd. All rights reserved.

doi:10.1016/j.carbon.2008.11.043

reduction [13–19]. Similar surface decomposition processes are also observed on noble metal surfaces [22,23]. There is evidence in the literature that soot is formed of polycyclic aromatic hydrocarbons (PAH) [24–28]. These PAHs are organized in layers that are stacked together forming a soot molecule as suggested by transmission electron microscopy and X-ray diffraction studies [29]. The surface properties of soot can be studied using a small PAH molecule. This is important because the computational time of density functional theory (DFT) calculations depends strongly on the size of the molecule. A first attempt to study the direct soot–NO interaction without catalysts using DFT was made by Kyotani and Tomita [30], but transition states (TS) and reaction rates were not reported in this work.

The purpose of this work is to clarify the non-catalytic interaction between soot and molecular nitric oxide. Different reaction pathways proposing the intermediate steps of the reactions (1)–(3) are presented. These two pathways describing the reduction of NO on a zigzag PAH surface are studied using DFT calculations, transition state theory and kinetic Monte-Carlo (kMC) simulations. The adsorption on a armchair PAH surface will be investigated in the future. The geometries of the transition states and the stable species were optimized. The energy, vibrational frequencies, and spin and bond populations of the geometry optimized species were also computed in these DFT calculations to determine the forward and backward reaction rate of each intermediate reaction using transition state theory. Finally, a kMC simulation at 560 °C employing the current rates and intermediate species demonstrates the conversion of NO into N₂ on a soot surface.

In the experimental section, the behavior of a soot particle with active carbon sites in a nitric oxide environment has been studied. It has been observed that the conversion of nitric oxide to nitrogen stops after a certain conversion level. The purpose of the experimental work is to validate our theoretical model.

2. DFT calculations

2.1. Calculation details

A naphthalene molecule with four unsaturated carbon atoms on which the nitric oxide molecule attaches represents the free radical carbon atoms of a soot surface for computational reasons. All the DFT calculations were performed using DMol3 which is included in the Materials Studio software package [31]. The generalized gradient approximation (GGA) corrected Hammett–Cohen–Tozer–Handy (HCTH) functional [32] was used. This functional has been fitted to a training set of 407 atomic and molecular systems [33]. The double numerical atomic orbital augmented by a polarized function basis set (DNP) that is comparable to the 6-31G** basis set was selected. All the calculations were performed with fine settings for calculation accuracy. The thresholds are: 1×10^{-5} Ha for the maximum energy change, 2×10^{-3} Ha/Å for the maximum force and 5×10^{-3} Å for the maximum displacement. Smearing was turned off for all the calculations except transition state 1: in this calculation, 0.004 Ha of smearing to the orbital occupation was applied to achieve electronic convergence. The single point energies of species

2 and species 3 used to determine the activation energy ΔE_{act} for the reaction from species 2 to species 3 and vice versa were also calculated with smearing to minimize the error. A geometry optimization was performed to determine the geometry of each stable species and the vibrational frequencies were calculated verifying that there are no imaginary frequencies. Transition states were verified by vibrational analysis. The optimizations were performed for different spin multiplicities. The multiplicity with the lowest energy and reasonable spin densities was chosen as proposed by Kyotani and Tomita [30]. It has been found that the zigzag sites are in a triplet state which is consistent with the findings of Radovic and Bockrath [34]. The bond population analysis was performed using the Mayer calculation method [35], which provides bond orders that are close to the corresponding classical values. The Mulliken spin population analysis [36] was applied to calculate the spin densities. The temperature dependent reaction rates $k(T)$ were calculated with transition state theory applying

$$k(T) = \frac{k_B T}{h} \frac{Q^\ddagger}{Q_A Q_B} \exp\left(\frac{-\Delta E_{act}}{k_B T}\right) \quad (4)$$

for bimolecular reactions and

$$k(T) = \frac{k_B T}{h} \frac{Q^\ddagger}{Q_A} \exp\left(\frac{-\Delta E_{act}}{k_B T}\right) \quad (5)$$

for unimolecular reactions. Q^\ddagger is the total partition function of the transition state, Q_A and Q_B are the partition functions of the reactants A and B and ΔE_{act} is the activation energy of the reaction. T is the temperature, h Planck's constant and k_B Boltzmann's constant. The total partition function is calculated as the product of the vibrational, translational, rotational and electronic partition functions. The reaction rates were calculated using transition state theory, with temperatures ranging from 20 to 2700 °C in 10 °C steps and a linear least-square fitting algorithm was used to fit the rate coefficients A , n and ΔE applying the modified Arrhenius expression:

$$k(T) = A \times \left(\frac{T}{T_0}\right)^n \times \exp\left(\frac{-\Delta E}{RT}\right) \quad (6)$$

where T_0 was set to 1 K.

2.2. Results

Two different reaction pathways were studied in order to clarify the intermediate reactions during the reduction of NO on a radical soot surface. Reaction pathways 1 and 2 can be described by the reactions (1) and (3), and (1) and (2), respectively. Both pathways start with a naphthalene molecule with four active sites (species 1) and two free NO molecules. The Mulliken spin population analysis of the active carbon atoms is either close to +1 or –1 confirming that each unsaturated carbon has a free electron. The pathways lead from naphthalene (species 1) and NO to molecular N₂ and oxidized carbon sites C(O) (species 6 and species 9). The CO desorption process as proposed in reaction (1) and (3) from the soot surface has been widely discussed in the literature [37,38,41,42] and is therefore not investigated in this study.

In the following section, the two reaction pathways are described in detail. The numbering of the C-atoms in the naphthacene molecule is shown in Fig. 1a.

2.2.1. Pathway 1

Fig. 1 shows the stable species together with the transition states of reaction pathway 1. The energy surface can be found in Fig. 2. Table 1 shows the enthalpy of the species in this pathway compared to the enthalpy of the starting point: a naphthacene molecule with four active carbon atoms (species 1) and two free NO molecules. Bond length and bond population details can be found in Table 2.

The two nitric oxide molecules attach with the N–O bond axis parallel to the edge of the naphthacene molecule without any reaction barrier on the surface. Two ring structures containing N and O on top of the naphthacene (species 2) are created. This exothermic reaction releases 963.7 kJ/mol and the N–O bond is stretched from 1.15 to 1.4 Å. The bond population

of the N–O bond diminishes from 2.05 to 1.07 indicating that the new bonds formed to the carbon atoms and the stretching of the bond length reduce the strength of the nitric–oxygen bond significantly. This low bond population facilitates the breakage of the N–O bond. An activation energy of 133.4 kJ/mol is necessary to break the N–O bond (TS 1) and to create species 3. A small smearing of 0.004 Ha has been used to achieve convergence for the calculation of transition state 1. The calculation difficulties were caused by the flat energy surface in this region. The energy difference between transition state 1 and stable species 3 is only 2.3 kJ/mol. After the first N–O bond is broken the bond between the oxygen atom and the carbon atom C(1) and the bond between the nitrogen atom and the carbon atom C(2) are fortified. The bond population of the nitrogen–carbon bond increases from 1.5 to 1.6 while the oxygen–carbon bond population increases from 1.1 to 1.7. The spin population of the nitrogen atom which is bound to the carbon atom C(4) is 1.4 indicating that there

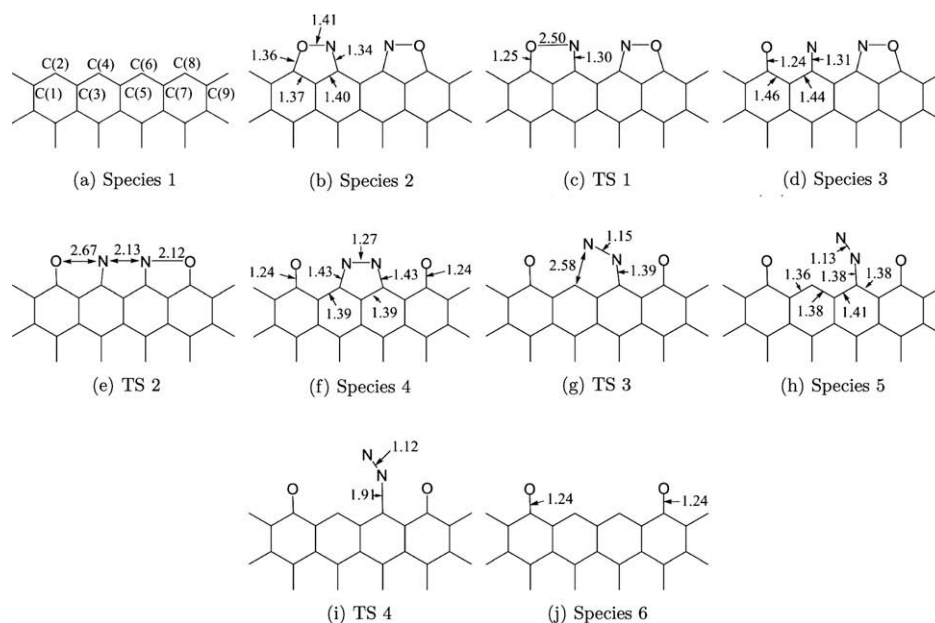


Fig. 1 – Stable species and transition states of reaction pathway 1. The numbers indicate the bond length in Å.

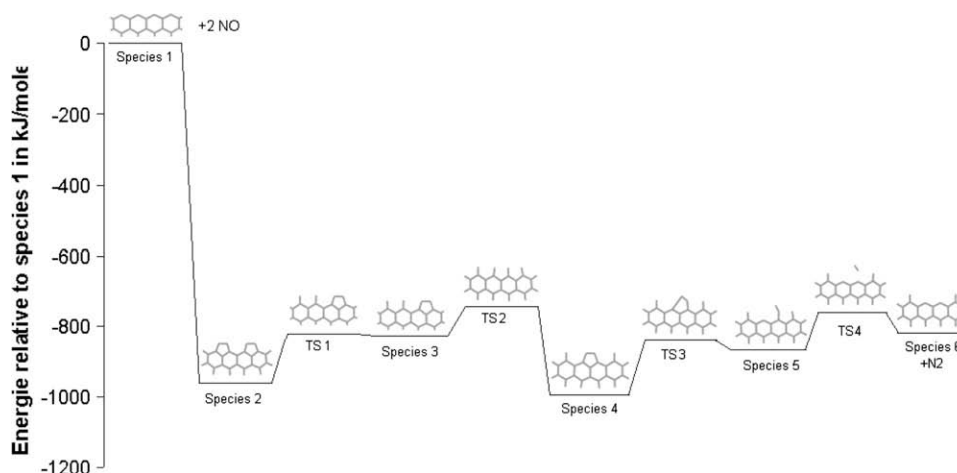


Fig. 2 – Energy surface of reaction pathway 1 in kJ/mol.

Table 1 – Enthalpy in kJ/mol of the species in reaction pathway 1 compared to species 1 and two nitric oxide molecules.

Structure	ΔH	
	Without smearing	With smearing
Species 1 + 2 NO	0	
Species 2	–963.7	–963.7
TS 1		–830.3
Species 3	–828.3	–832.6
TS 2	–740.5	
Species 4	–994.6	
TS 3	–843.1	
Species 5	–867.0	
TS 4	–758.5	
Species 6	–794.5	

are unbound electrons. This radical nitrogen atom facilitates the breakage of the bond between the other nitrogen and oxygen atoms because it attracts the second nitrogen atom. This second N–O bond is broken with an activation energy of 87.8 kJ/mol (TS 2) and a bond between the two nitrogen atoms is formed (species 4). The bond population of the N–N bond is 1.75. The bond between the nitrogen and the carbon atoms is degraded by the strong N–N bond and the first of the two N–C

Table 2 – Bond length in Å and Mayer bond population for reaction pathway 1.

Species	Bond	Length in Å	Population
Species 1	C(1)–C(2)	1.35	1.55
	C(2)–C(3)	1.40	1.24
	C(3)–C(4)	1.37	1.38
	C(4)–C(5)	1.38	1.31
Species 2	C(1)–C(2)	1.39	1.28
	C(2)–C(3)	1.37	1.26
	C(3)–C(4)	1.40	1.14
	C(4)–C(5)	1.42	1.12
	C(2)–O	1.36	1.06
	N–O	1.41	1.08
	C(4)–N	1.34	1.47
Species 3	C(1)–C(2)	1.45	1.12
	C(2)–C(3)	1.46	1.08
	C(3)–C(4)	1.44	1.11
	C(4)–C(5)	1.45	1.11
	C(2)–O	1.24	1.70
	C(4)–N	1.31	1.61
Species 4	C(3)–C(4)	1.39	1.33
	C(4)–C(5)	1.39	1.19
	C(4)–N	1.43	1.10
	N–N	1.27	1.75
Species 5	C(5)–C(6)	1.41	1.17
	C(6)–C(7)	1.38	1.26
	C(6)–N	1.38	1.02
	N–N	1.32	2.45
Species 6	C(1)–C(2)	1.45	1.10
	C(2)–C(3)	1.47	1.03
	C(3)–C(4)	1.36	1.43
	C(4)–C(5)	1.38	1.29
	C(2)–O	1.24	1.77

bonds can be broken with an energy of 151.5 kJ/mol (TS 3). The activation energy required to break the second bond and so to release molecular nitrogen from the structure is 108.5 kJ/mol (TS 4).

2.2.2. Pathway 2

Figs. 3 and 4 present the stable species and transition states as well as the energy surface of reaction pathway 2. The bond length and population details are presented in Table 3. The enthalpy of the different species is presented in Table 4. This pathway is shorter than pathway 1 and only three neighboring active carbon sites are necessary. In order to compare the results of pathway 2 with pathway 1 the same starting configuration has been chosen. In the first reaction step, the first NO molecule adsorbs with the N–O bond axis parallel to the soot surface forming a 5-member ring (species 7) as in reaction pathway 1, but in contrast to pathway 1 the second NO molecule adsorbs with the oxygen atom down on the radical carbon atom next to the already adsorbed nitrogen atom. This single site adsorption is energetically less stable than the NO adsorption on two sites, but the decreasing number of available sites during the reaction due to active site-blocking increases the importance of this reaction pathway. A discussion about active site-blocking can be found in the review of Aarna and Suuberg [7]. A bond between the two nitrogen atoms is formed and both nitrogen–oxygen bonds are broken in the same step (species 8). The activation energy of this reaction is 12.7 kJ/mol (TS 5). The bond populations are close to the values of reaction pathway 1. The activation energy required to release the N₂ molecule from the soot surface is 96.3 kJ/mol (TS 6). The N₂ abstraction reaction of pathway 2 needs less energy than the similar reaction of pathway 1 because the enthalpy of species 5 is 9.8 kJ/mol less than the enthalpy of species 8.

2.2.3. Reaction rates

The forward and backward reaction rates have been calculated using transition state theory and a linear least-square fitting algorithm was used to determine the parameters A , n and ΔE (see Eq. 6). The reaction rate for the barrier-less NO absorption reaction has not been calculated because variational transition state theory is needed to calculate the reaction rate of barrier-less reactions. This reaction should be very fast compared to the other rates as indicated by experiments and therefore the rate can be neglected. The forward and backward reaction rate of the reaction from species 2 to species 3 has been calculated with 0.004 Ha of smearing for the transition state. In order to minimize the error, the activation energy of the reactants of this single reaction was also calculated with the same smearing. All the other reaction rates were calculated without smearing. The Arrhenius parameters for pathway 1 can be found in Table 5 and for pathway 2 in Table 6.

3. Experimental work

Detailed information about the experimental study can be found in [4]. In this paper only the important parts that consider the direct soot NO interaction are summarized.

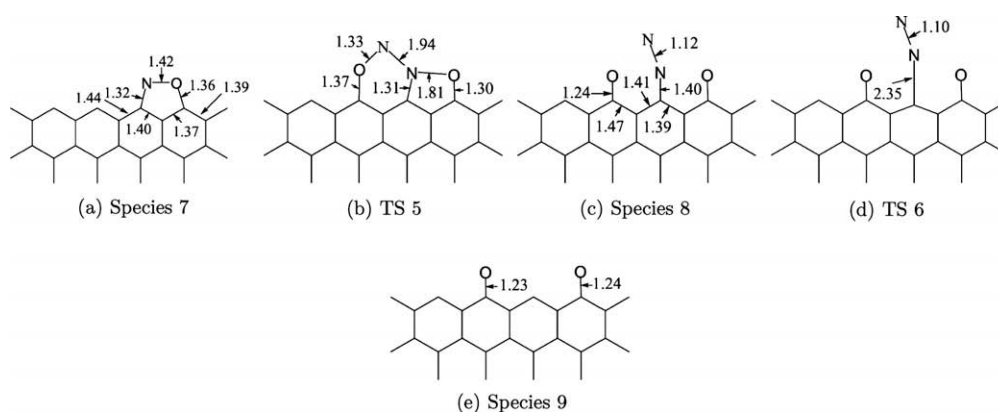


Fig. 3 – Stable species and transition states of reaction pathway 2. The numbers indicate the bond length in Å.

3.1. Setup

For the experimental examination of the soot/NO reaction a self-prepared carbon black is taken. This model soot is made by employing a C_3H_6/O_2 diffusion burner. Detailed data on preparation and characterization as well as on study of the reaction of soot with NO have already been described elsewhere [4]. Thus, only a brief description of the physical-chemical properties of the soot (Table 7) and the experimental approach is given here. In the first stage of the reaction, the soot is activated at 560 °C by O_2 (5.0 vol.% O_2 , 95 vol.% Ar), while in the 2nd step the dosage of O_2 is stopped and the sample is flushed with Ar. Hereby, surface oxygen compound originated from O_2 exposure desorb thermally thus forming active C sites on the soot. After complete desorption of CO_x , the 3rd regime is started by switching to a blend of 500 ppm NO in Ar. In the final period, the remaining soot is oxidised by dosing a mixture of 5.0 vol.% O_2 and 95 vol.% Ar while heating to ca. 715 °C at the rate of 10 K/min.

3.2. Results

The experimental results are presented in Fig. 5. An enlarged graph can be found in Fig. 6 to clarify the experimental observations directly after the NO exposure. This graph shows that the NO molecules adsorb on the active carbon sites instantaneously. NO does not remain in the surrounding gas in the first 20 s of NO exposure. The amount of NO in the surrounding gas increases rapidly after the active carbon sites are saturated. N_2 and a small amount of CO are formed directly after the NO exposure. The amount of N_2 released from the soot is less than the amount of NO consumed, confirming there is a portion of NO trapped on the soot surface. This is consistent with other experimental results [7]. After the reaction stops a significant amount of nitric oxide ranging from 40% to 63% remains on the soot surface. The TPO after the NO exposure oxidizes the soot entirely and releases N_2 in addition to NO, CO and CO_2 confirming that some NO molecules have been bound to the soot molecule. These experimental results are used to validate our theoretical model.

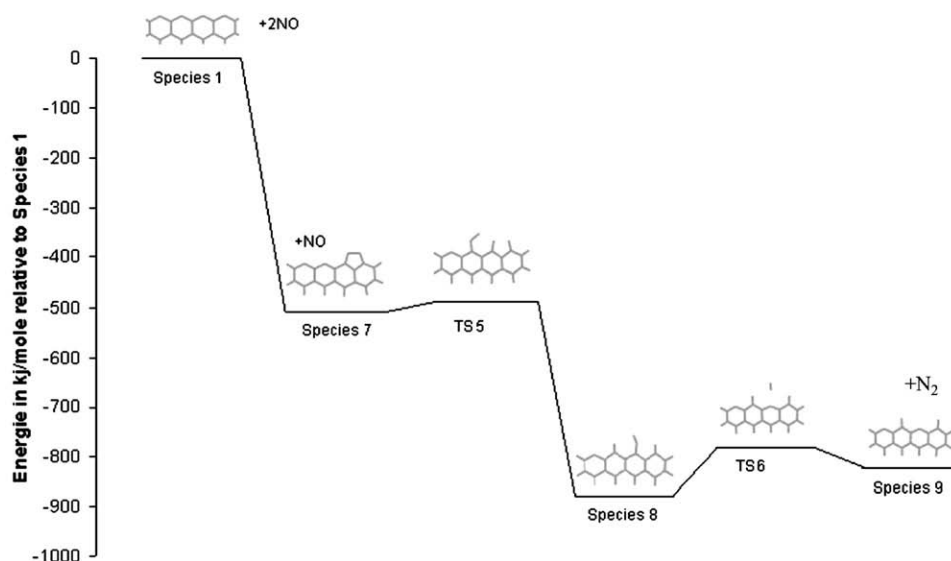


Fig. 4 – Energy surface of reaction pathway 2 in kJ/mol.

Table 3 – Bond length in Å and Mayer bond population for reaction pathway 2.

Species	Bond	Length in Å	Population
Species 7	C(5)–C(6)	1.44	1.05
	C(6)–C(7)	1.41	1.15
	C(7)–C(8)	1.37	1.26
	C(8)–C(9)	1.40	1.27
	C(6)–N	1.32	1.54
	N–O	1.41	1.06
	C(9)–O	1.36	1.08
Species 8	C(3)–C(4)	1.47	1.05
	C(4)–C(5)	1.47	1.07
	C(4)–O	1.24	1.76
	C(5)–C(6)	1.40	1.24
	C(6)–C(7)	1.39	1.25
	C(6)–N	1.40	0.98
	N–N	1.12	2.52
Species 9	C(3)–C(4)	1.49	1.01
	C(4)–C(5)	1.46	1.05
	C(7)–C(8)	1.46	1.05
	C(8)–C(9)	1.46	1.09
	C(4)–O	1.23	1.83
	C(8)–O	1.24	1.77

4. kMC simulations

4.1. Calculation details

The present study utilizes a detailed Monte-Carlo model, called the kinetic Monte-Carlo-Aromatic Site (kMC-ARS) model, to study the oxidation of PAHs present in soot particles in a nitric oxide–argon (NO–Ar) environment. The kMC-ARS model is based on the processes involved in the two pathways for soot oxidation described above, along with some processes taken from [42,41] as shown in Table 8.

These PAH processes are allowed to take place on a substrate PAH molecule. In this work, a substrate rich in zig-zag sites was chosen (Fig. 7a) based on the findings of Weilmünster et al. [39] and Raj et al. [40]. Weilmünster suggests that the mature PAHs (present at higher heights above the burner (HABs) in flames) are rich in zig-zag and free-edge sites. Therefore, it can be assumed that the PAHs present in mature soot particles would also be rich in these sites. The different reaction steps are shown in Table 8. After a process takes place on the substrate, the kMC-ARS model determines the resulting structure of the substrate molecule based on the positions of C, N and O atoms and the relative positions of

Table 4 – Enthalpy of the species in reaction pathway 2 compared to species 1 and two nitric oxide molecules.

Structure	ΔH in kJ/mol
Species 1 + 2 NO	0
Species 7 + NO	–503.8
TS 5 + NO	–491.1
Species 8	–876.8
TS 6	–780.5
Species 4	–818.3

the reactive sites. A full description of this model can be found in [40]. This work involves the simulation of the oxidation of a PAH molecule by NO (see Section 4). The substrate is assumed to be at the same temperature as the gas-phase environment which is equal to 560 °C. The pressure and NO concentration are taken to be 1 atm and 500 ppm, respectively. These conditions are assumed to remain unchanged throughout the simulation. The stochastic algorithm developed to track the structure of PAHs after each reaction step is detailed in [40] and is briefly reviewed here. The process of PAH oxidation by NO is modeled as a Markovian sequence of reaction events [43]. The outcome of this model depends on the concentration of reacting species, the rates of the possible reaction events and the probability of a reaction being chosen. The rates for the processes listed in Table 8 are calculated by

$$R_i = k_i \times C_s \times N_{site}, \quad i = 1, 2, \dots, I$$

where I is the number of processes in Table 8, C_s is the concentration of chemical species involved in the bimolecular reactions and N_{site} is the number of reactive sites on the PAH molecule involved in the process i . At time t , an exponentially distributed waiting time for a reaction to take place τ with parameter λ is calculated where λ is the sum of all the process rates

$$\lambda = \sum_{i=1}^I R_i$$

$t = t + \tau$ gives the time for the next reaction. A reaction is chosen based on the probability calculated using its reaction rate. A site of correct type is chosen uniformly assuming all sites to be equally probable. The substrate structure is then updated based on the chosen process and the above procedure is repeated for the desired simulation time. The results obtained from the simulations are discussed in the next section.

4.2. kMC results

As mentioned in Section 4 the complete oxidation of soot takes place in four stages: partial oxidation of soot in an O₂–Ar environment; removal of CO in Ar environment to create radical sites on the soot surface; exposure of soot particles with radical sites to NO–Ar environment where NO molecules get deposited on the soot surface with some removal of N₂ and CO (partial oxidation); further oxidation of

Table 5 – Arrhenius parameters for reaction pathway 1. A in (1/s) for unimolecular reactions and cm³/(mol s) for bimolecular reactions, ΔE in kJ/mol. Bimolecular reactions are marked with an asterisk.

Reaction	A	n	ΔE
2 → 3	2.2×10^{13}	0.34	127.3
3 → 2	1.8×10^{12}	0.10	1.5
3 → 4	1.8×10^{12}	0.44	78.7
4 → 3	1.0×10^{12}	0.45	244.0
4 → 5	9.3×10^{12}	0.23	148.1
5 → 4	3.2×10^{12}	0.07	23.6
5 → 6	2.0×10^{13}	0.11	108.6
6 → 5	1.7×10^3	2.51	38.9*

Table 6 – Arrhenius parameters for reaction pathway 2. A in (1/s) for unimolecular reactions and cm³/(mol s) for bimolecular reactions, ΔE in (kJ/mol). Bimolecular reactions are marked with an asterisk.

Reaction	A	n	ΔE
7 → 8	3.2×10^2	2.62	11.0*
8 → 7	6.7×10^{11}	0.27	379.9
8 → 9	3.6×10^{13}	0.4	89.3
9 → 8	2.5×10^3	2.65	35.3*

Table 7 – Physical-chemical properties of the used C₃H₆ soot.

BET surface area	91 m ² /g
Amount of adsorbed species	2.6 wt.%
Chemical composition ^{a,b}	98.8 wt.% C, 0.7 wt.% O, 0.5 wt.% H
Diameter of primary particles	20–100 nm

a The amount of adsorbed species is neglected.

b The soot is ashless.

soot in an O₂-Ar environment. In this work only the third stage of this oxidation has been simulated assuming the substrate to be full of radical sites because detailed reaction pathways showing the interaction of O₂ with PAHs were not considered in this work and will be investigated in the a future study. The reaction rate of reaction 1 (Table 8) has been assumed to be infinitely fast. This implies that the substrate would be uniformly populated with NO molecules at the beginning of the simulations. Fig. 7b shows a computed PAH molecule obtained after a real time simulation of 0.15 s in a NO-Ar environment. It was noticed that the addition of NO onto the soot surface subsequently leads to the removal of C atoms in the form of CO or HCCO through reactions 8–10 (Table 8). Fig. 8 shows the number of reaction events normalized by the number of C atoms on the substrate molecule after a real time simulation of 0.15 s, averaged over 100 simulation runs. It can be noticed in this figure that reaction 5 involved in pathway 1 takes place less frequently than reaction

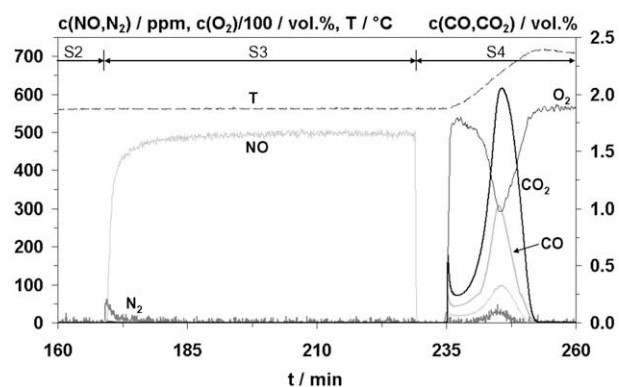


Fig. 5 – Concentration of CO, CO₂, O₂, NO and N₂ and the temperature as a function of time. Si represents the ith stage in soot oxidation.

Table 8 – PAH processes used in the kMC simulations. The units of T and R are K and kJ/(mol K), respectively. The rate constants for reactions 8–10 has been taken from [42,41].

No.	Process	Rate constant, k
1		Infinitely fast
2		$2.2 \times 10^{13} T^{0.34} e^{-\frac{127.3}{RT}}$
3		$1.8 \times 10^{12} T^{0.44} e^{-\frac{79.7}{RT}}$
4		$9.3 \times 10^{12} T^{0.23} e^{-\frac{148.1}{RT}}$
5		$2.0 \times 10^{13} T^{0.11} e^{-\frac{108.6}{RT}}$
6		$3.2 \times 10^2 T^{2.62} e^{-\frac{11}{RT}}$
7		$3.6 \times 10^{13} T^{0.4} e^{-\frac{89.3}{RT}}$
8		$7.4 \times 10^{11} e^{-\frac{92.3}{RT}}$
9		$7.4 \times 10^{11} e^{-\frac{92.3}{RT}}$
10		$7.4 \times 10^{11} e^{-\frac{92.3}{RT}}$

7 involved in pathway 2. This implies that pathway 2 contributes more to the formation of N₂ molecules than pathway 1 as pathway 1 requires the presence of two adjacent N atoms and this may not occur very frequently. As the reaction progresses the resulting PAH structure develops bay-type structures prohibiting further addition of NO on PAHs using with the present reaction pathway. Additionally, it can be noticed in Fig. 7b that there are a number of N and O atoms on PAH edges which cannot be removed. Therefore no further oxidation of PAHs with NO molecules can take place after some fixed time. These results are qualitatively in agreement with the experimental observations. Experimentally observed concentration profiles of NO, CO and N₂ in stage 3 (see Fig. 5) show that addition of NO on the soot surface along with the removal of N₂ and CO takes place in the early stages of the experiment (before 173 min). Thereafter the concentration of NO becomes almost constant indicating negligible

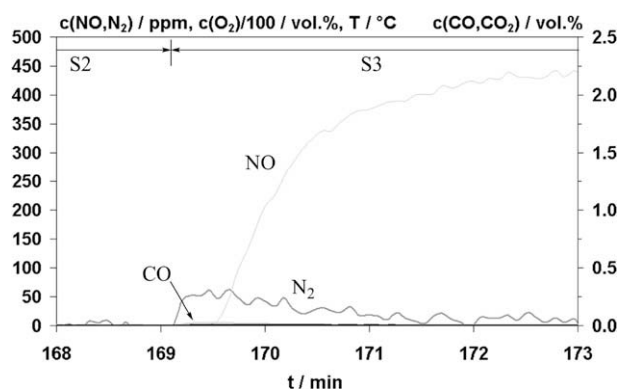


Fig. 6 – Concentration of CO, CO₂, O₂, NO and N₂ and the temperature as a function of time shortly before and after the NO exposure.

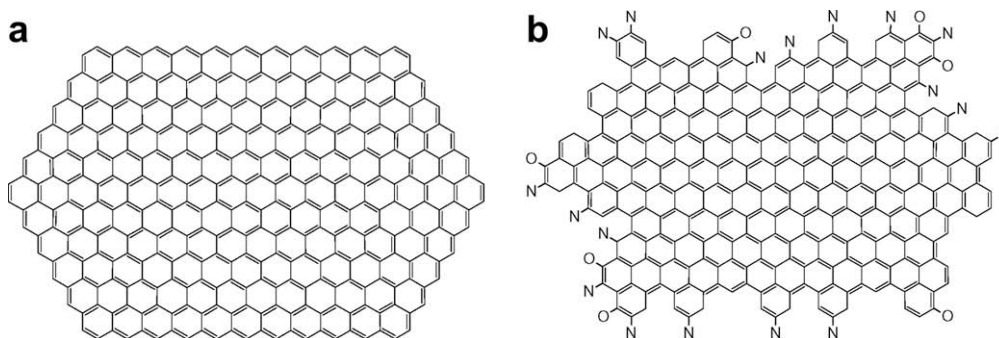


Fig. 7 – (a) An example PAH substrate. (b) An example computed PAH obtained after a simulation of 0.15 s.

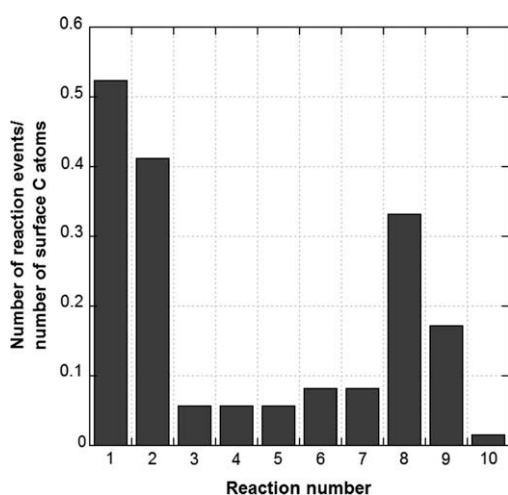


Fig. 8 – Average number of reaction events normalised with the number of surface carbon atoms on the substrate PAH after a real time simulation of 0.15 s. The reactions corresponding to the reaction numbers (on x-axis) can be obtained from Table 8.

oxidation of soot particles by NO. It is difficult to make any quantitative comparison as there might be many other reactions taking place on PAH edges, for example the addition of NO on bay sites and oxidation of phenalene-like structures (see Fig. 7b) during the oxidation. Also, a number of stable intermediates are possible such as embedded N atoms in the PAHs, which cannot occur with the present reaction mechanism. The above arguments clearly indicate the need to extend the reaction mechanism proposed in this work (Table 8).

5. Conclusions

Two different reaction pathways leading from a soot molecule with a surface containing radical carbon atoms and nitric oxide in the surrounding gas to oxidized soot and molecular N_2 were explored using quantum mechanical calculations. The computed reaction rates and species were used in a kMC simulation. The theoretical results qualitatively agree with the experimental observations. Fig. 8 shows that reac-

tion pathway 2 (reaction number 6, 7) is slightly preferred to pathway 1 (reaction number 3, 4, 5) although pathway 2 contains the energetically less favorable single site adsorption of NO. The decreasing number of free radical sites during the reaction due to blocked carbon atoms prevents the adsorption of NO on two neighboring sites. The different reaction steps in each pathway occur the same number of times. This demonstrates that once the nitric oxide molecules are bound to the soot surface and the alignment allows further reactions to proceed, N_2 is formed quickly. This is consistent with the experimental observations (see Fig. 6) where the NO exposure in the third experimental stage leads to an immediate N_2 production. Hence, the kMC results based on a DFT derived reaction mechanism presented herein are able to describe the experimental observations.

Fig. 7b clarifies the reasons why a portion of NO remains trapped on the soot surface. The calculations demonstrate that the alignment of the nitric oxide molecules is crucial. Two NO molecules attached to the surface in the 'wrong' direction (N–O–N–O) block the active carbon sites and remain trapped on the soot molecule as seen in the lower left edge of the soot molecule in Fig. 7b. The vacancies created by CO desorption processes inhibit subsequent decomposition of NO molecules on the surface. Nevertheless NO can adsorb on the vacancies as found by Kyotani and Tomita [30] but this leads to very stable structures and hence further decomposition is unlikely at 560 °C. The importance of the correct alignment, in addition to the holes created by CO desorption processes, and the trapped oxygen and nitrogen atoms on the soot surface explain why the reaction ceases and the low amount of N_2 and CO formed in the third experimental stage. There are also other reactions and pathways between soot and NO possible however, the influence of these reactions is likely to be negligible based on the fact that our theoretical investigations are consistent with experimental observations.

In the current study, we consider only the forward reaction processes in our kMC simulations, but it has been demonstrated that the initial adsorption position and geometry of the nitric oxide molecules on the soot surface is the crucial part of the reaction. The desorption of NO from the soot surface is negligible because the activation energy is much higher than the dissociation energy. This is confirmed by experiments where NO is not released from the surface before increasing the temperature significantly. As the reaction rate is mainly determined by the sterics of the adsorption process,

the backward reactions are likely to have only a minor effect. Therefore we can summarize that our reaction pathways and kMC simulations describe qualitatively the experimental observations.

This study represents the first comprehensive theoretical investigation of the reaction mechanism of the non-catalytic soot reduction by NO. A combination of a mechanistic DFT study and a kMC study based thereon enabled a qualitative description of the experimental results of the soot reduction by NO. In the future, we will add the backward reactions to the kMC simulations in addition to some other reactions on different site geometries and try to explain the experimental findings in the fourth experimental stage at higher temperatures and in an oxygen rich environment.

Acknowledgements

Support from EPSRC Grant EP-C547241-1 is gratefully acknowledged. The useful discussions with Dr. Ivo Hermans are gratefully acknowledged.

REFERENCES

- Twigg M. Progress and future challenges in controlling automotive exhaust gas emissions. *Appl Catal B* 2007;20:2–15.
- Balle P, Bockhorn H, Geiger B, Jan N, Kureti S, Reichert D, et al. Study on the mechanism of the catalytic conversion of NO_x and soot into N₂ and CO₂ on Fe₂O₃ in diesel exhaust. *Chem Eng Process* 2006;45:1065–73.
- Carabineiro SA, Fernandes FB, Ramos AM, Vital J, Silva IF. Vanadium as a catalyst for NO, N₂O and CO₂ reaction with activated carbon. *Catal Today* 2000;57:305–12.
- Reichert D, Bockhorn H, Kureti S. Study of the reaction of NO_x and soot on Fe₂O₃ catalyst in excess of O₂. *Appl Catal B* 2008;80:248–59.
- Bockhorn H, Kureti S, Reichert D. Study on the mechanism of the catalytic conversion of NO_x and soot into N₂ and CO₂ on Fe₂O₃ in diesel exhaust. *Top Catal* 2007;42:283–6.
- Thomas K. The release of nitrogen oxides during char combustion. *Fuel* 1997;76:457–73.
- Aarna I, Suuberg E. A review of the kinetics of the nitric oxide–carbon reaction. *Fuel* 1997;76:475–91.
- De Soete G. Heterogeneous N₂O and NO formation from bound nitrogen atoms during coal char combustion. *Proc Combust Inst* 1990;23:1257–64.
- Rodriguez-Mirasol J, Ooms A, Pels J, Kapteijn F, Moulijn J. NO and N₂O decomposition over coal char at fluidized-bed combustion conditions. *Combust Flame* 1994;99:499–507.
- Teng H, Suuberg E, Calo J. Studies on the reduction of nitric oxide by carbon: The nitric oxide–carbon gasification reaction. *Energy Fuel* 1992;6:398–406.
- Yamashita H, Tomita A, Yamada A, Kyotani T, Radovic LR. Influence of char surface chemistry on the reduction of nitric oxide with chars. *Energy Fuel* 1993;7:85–9.
- Suzuki T, Kyotani T, Tomita A. Study on the carbon–nitric oxide reaction in the presence of oxygen. *Ind Eng Chem Res* 1994;33:2840–5.
- Illán-Gómez MJ, Linares-Solano A, Salinas-Martínez de Lecea C. NO reduction by activated carbons. 1. The role of carbon porosity and surface area. *Energy Fuel* 1993;7:146–54.
- Illán-Gómez MJ, Linares-Solano A, Radovic LR, Salinas-Martínez de Lecea C. NO reduction by activated carbons. 2. Catalytic effect of potassium. *Energy Fuel* 1995;9:97–103.
- Illán-Gómez MJ, Linares-Solano A, Radovic LR, Salinas-Martínez de Lecea C. NO reduction by activated carbons. 3. Influence of catalyst loading on the catalytic effect of potassium. *Energy Fuel* 1995;9:104–11.
- Illán-Gómez MJ, Linares-Solano A, Radovic LR, Salinas-Martínez de Lecea C. NO reduction by activated carbons. 4. Catalysis by Calcium. *Energy Fuel* 1995;9:112–8.
- Illán-Gómez MJ, Linares-Solano A, Radovic LR, Salinas-Martínez de Lecea C. NO reduction by activated carbons. 5. Catalytic effect of iron. *Energy Fuel* 1995;9:540–8.
- Illán-Gómez M J, Linares-Solano A, Radovic LR, Salinas-Martínez de Lecea C. NO reduction by activated carbons. 6. Catalysis by transition metals. *Energy Fuel* 1995;9:976–83.
- Illán-Gómez M, Linares-Solano A, Radovic LR, Salinas-Martínez de Lecea C. NO reduction by activated carbons. 7. Some mechanistic aspects of uncatalyzed and catalyzed reaction. *Energy Fuel* 1995;9:104–11.
- Chambrión P, Kyotani T, Tomita A. Role of N-containing surface species on NO reduction by carbon. *Energy Fuel* 1998;12:416–21.
- Chambrión P, Orikasa H, Kyotani T, Tomita A. A study of the C–NO reaction by using isotopically labelled C and NO. *Fuel* 1997;76:493–8.
- Inderwildi OR, Jenkins SJ, King DA. An unexpected pathway for the catalytic oxidation of Methylidyne on Rh[111] as a route to syngas. *J Am Chem Soc* 2007;129:1751–9.
- Inderwildi OR, Jenkins SJ, King DA. Dynamic interplay between diffusion and reaction: Nitrogen recombination on Rh[2 1 1] in car exhaust catalysis. *J Am Chem Soc* 2008;130:2213–20.
- Frenklach M. Method of moments with interpolative closure. *Chem Eng Sci* 2002;57:2229–39.
- Singh J, Patterson RIA, Kraft M, Wang H. Numerical simulation and sensitivity analysis of detailed soot particle size distribution in laminar premixed ethylene flames. *Combust Flame* 2006;145:117–27.
- Balthasar M, Kraft M. A stochastic approach to solve the particle size distribution function of soot particles in laminar premixed flames. *Combust Flame* 2003;133:289–98.
- Singh J, Balthasar M, Kraft M. Stochastic modeling of soot particle size and age distributions in laminar premixed flames. *Proc Combust Inst* 2005;30:1457–65.
- Patterson RIA, Kraft M. Models for the aggregate structure of soot particles. *Combust Flame* 2007;151:160–72.
- Chen HX, Dobbins RA. Crystallography of particles formed in hydrocarbon combustion. *Combust Sci Technol* 2000;159:109–28.
- Kyotani T, Tomita A. Analysis of the reaction of carbon with NO/N₂O using ab initio molecular orbital theory. *J Phys Chem B* 1999;103:3434–41.
- Delly B. An all-electron numerical method for solving the local density functional for polyatomic molecules. *J Chem Phys* 1990;92:508–17.
- Hambrecht FA, Cohem AJ, Tozer AJ, Handy NC. Development and assessment of new exchange–correlation functionals. *J Chem Phys* 1998;109:6264–71.
- Boese AD, Handy NC. A new parametrization of exchange–correlation generalized gradient approximation functionals. *J Chem Phys* 2001;114:5497–503.
- Radovic LR, Bockrath B. On the chemical nature of graphene edges. Origin of stability and potential for magnetism in carbon materials. *J Am Chem Soc* 2005;127:5917–27.
- Mayer I. Bond orders and valences from ab initio wave functions. *Int J Quantum Chem* 1986;29:477–83.
- Mulliken R. Electronic population analysis on LCAO–MO molecular wave functions. I. *J Chem Phys* 1955;23:1833–46.

- [37] Zhu ZH, Lu GQ. New insights into NO–carbon and N₂O–carbon reactions from quantum mechanical calculations. *Energy Fuel* 2003;17:1057–61.
- [38] Sendt K, Haynes BS. Density functional study of the chemisorption of O₂ on the zig-zag surface of graphite. *Combust Flame* 2005;143:629–43.
- [39] Weilmünster P, Keller A, Homann KH. Large molecules, radicals, ions and small soot particles in fuel-rich hydrocarbon flames part I: Positive ions of polycyclic aromatic hydrocarbons(PAH) in low-pressure premixed flames of acetylene and oxygen. *Combust Flame* 1999;116:62–83.
- [40] Raj A, Celnik MS, Shirley RA, Sander M, Patterson RIA, West RH, et al. A statistical approach to develop a detailed soot growth model using PAH characteristics. Technical Report 52, C4e-Preprint Series, Cambridge, 2007. Available from: <http://como.cheng.cam.ac.uk>.
- [41] Frank P, Herzler J, Just T, Wahl C. High-temperature reactions of phenyl oxidation. *Proc Combust Inst* 1994;25:833–40.
- [42] Wang H, Frenklach M. A detailed kinetic modeling study of aromatic formation in laminar premixed acetylene and ethylene flames. *Combust Flame* 1997;110:173–221.
- [43] Frenklach M. On surface growth mechanism of soot particles. *Proc Combust Inst* 1996;26:2285–93.